Atomic Force Microscopy Study of the Effects of Mg 2+ and Other Divalent Cations on the End-to-End DNA Interactions †

ARTICLE *in* BIOCHEMISTRY · OCTOBER 2002

Impact Factor: 3.02 · DOI: 10.1021/bi026102e · Source: PubMed

2 AUTHORS, INCLUDING:

Yuri L. Lyubchenko
University of Nebraska Medical Center
192 PUBLICATIONS **5,621** CITATIONS

SEE PROFILE

Atomic Force Microscopy Study of the Effects of Mg^{2+} and Other Divalent Cations on the End-to-End DNA Interactions†

Paul R. Dahlgren and Yuri L. Lyubchenko*

Department of Microbiology, Arizona State University, Tempe, Arizona 85287-2701

Received May 8, 2002; Revised Manuscript Received July 19, 2002

ABSTRACT: Atomic force microscopy (AFM) was applied to directly visualize the end-to-end DNA interaction mediated by magnesium cations. We took advantage of the APS-mica, allowing the preparation of samples in a broad range of monovalent and divalent cations to separate the effects of Mg^{2+} and Na^+ cations on the interaction of restriction DNA fragments with cohesive end. The AFM data clearly show that DNA restriction fragments with cohesive ends form substantial amount of circles in the presence of Mg^{2+} cations, suggesting that Mg^{2+} cations stabilize the interaction of cohesive ends. This effect depends on the $MgCl_2$ concentration, so that the yield of circles approaches 18% in the presence of 50 mM $MgCl_2$. Furthermore, we demonstrate that this conferred cohesive end stability is specific for divalent cations, as substitution of $MgCl_2$ with NaCl leads to a near complete loss of cohesive end stability. We further demonstrate that cohesive end stabilization is achieved by substituting Mg^{2+} with Ca^{2+}, Mn^{2+}, or Zn^{2+}. The data obtained suggest that the end stabilization mediated by divalent cations is primarily the result of inter-base interactions rather than bridging of phosphate moieties.

It has been reported that Mg^{2+} helps stabilize several different types of DNA structures such as four- and three-way junctions [*1* and references therein, *2*] and PyPuPu triplexes (*3*). Furthermore, a few studies have shown that Mg^{2+} can induce bending in DNA containing GGGCCC segments (*4*) and enhance curvature in DNA contain A-tracts (*5*−*7*). Additionally, DNA modifying enzymes such as DNA ligase require Mg^{2+} to function. This requirement for Mg^{2+} may be 2-fold: first, it is utilized as a cofactor in catalysis, but not so obvious is the fact that it may be used to stabilize DNA end interactions.

A recent study by Révet and Fourcade, for the first time, demonstrated that Mg^{2+} cations with uranyl acetate help stabilize end-to-end interactions in cohesive end DNA fragments regardless of their size in the absence of DNA ligase (*8*). They directly visualized their results with atomic force microscopy (AFM) utilizing UO_2^{2+} in conjunction with Mg^{2+} during the deposition of their samples. It is unclear if Mg^{2+} or other divalent cations are solely responsible for their observed effect and if the effect is concentration dependent.

In this study we utilized AFM to investigate the specific effect of Mg^{2+} in the absence of uranyl acetate on the structure of specific linear DNA fragments. We took advantage of APS-mica (*9*) based surface technology, which allows for the deposition of samples without the requirement of Mg^{2+}. We conducted several experiments comparing the effect of Mg^{2+} concentration with two 415 bp fragments, one with cohesive ends and one with blunt ends, and a 441 bp blunt end fragment. We also compared the effect of Mg^{2+} to that of Na^+ on the cohesive ends stability. We further studied the end-stabilization effect of other divalent cations (Ca^{2+}, Mn^{2+}, and Zn^{2+}), which revealed a stronger effect for cations with predominant affinity for DNA bases.

MATERIALS AND METHODS

Plasmid and Linearized DNA. Reid C. Johnson, UCLA, provided the plasmid pRJ1199, and Vladimir N. Potaman, Texas A&M U, provided additional pRJ1199. Both Hind III and EcoRV (New England Biolabs) digests of pRJ1199 yielded two fragments (large fragment ∼4.3 kb and small ∼415 bp). For AFM experiments the 415 bp fragments from both digests were isolated and purified using Ultraclean 15 kit from MioBio (Solana Beach, CA) (*10*). François Strauss, Institut Jacques Monod, Paris, France, provided the 441 bp blunt end fragment.

AFM Procedure. All three fragments (0.5−1 μg/mL) were incubated with various concentrations of $MgCl_2$ (3, 6, 10, and 50 mM) and 1 mM EDTA (no $MgCl_2$) in 10 mM Tris−HCl pH 7.9 and 50 mM NaCl and incubated at 30 °C for 15 min. Similarly, both 415 bp fragments (0.5−1 μg/mL) were incubated with 250 mM NaCl in 10 mM Tris−HCl pH 7.9) at 30 °C for 15 min. The 415 bp cohesive end fragment (0.5−1 μg/mL) was incubated with various concentrations of divalent cations: $CaCl_2$ (3, 6, and 10 mM) in 10 mM Tris−HCl pH 7.9 and 50 mM NaCl, $MnCl_2$ (3, 6, and 10 mM) in 10 mM HEPES−HCl pH 7.0 and 50 mM NaCl, and $ZnCl_2$ (3, 6, and 10 mM) in 10 mM acetate−HCl pH 5.5 and 50 mM NaCl. For controls, the 415 bp cohesive end fragment (0.5−1 μg/mL) was incubated in two buffers: 1 mM EDTA (no $CaCl_2$ or $MnCl_2$) in 10 mM HEPES−HCl pH 7.0 and 50 mM NaCl, and 1 mM EDTA (no $ZnCl_2$) in 10 mM acetate−HCl pH 5.5 and 50 mM NaCl. All divalent cation samples and subsequent controls were incubated at 30 °C for 15 min before deposition. For imaging in air, 4.5

† This work was supported by NIH Grant GM 622235 (Y.L.L.).

* Corresponding author. Address: Department of Microbiology, Arizona, State University, P.O. Box 85287-2701, Tempe, AZ 85287-2701. Tel: (480) 965-8430. E-mail: yuri.lyubchenko@asu.edu.

10.1021/bi026102e CCC: $22.00
Published on Web 08/28/2002

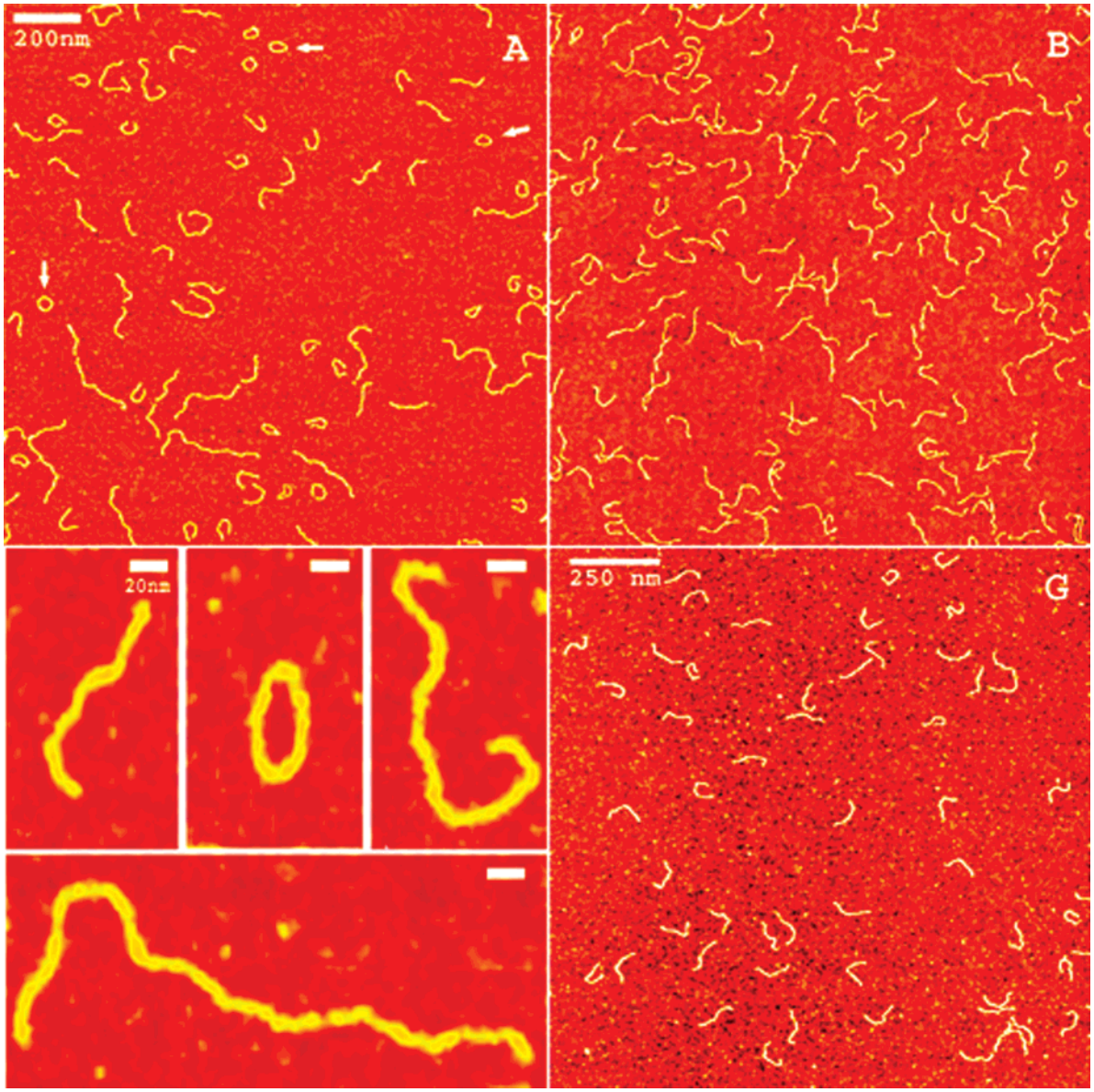

FIGURE 1: AFM images showing the effects of Mg^{2+} on both blunt and cohesive end DNA fragments. (A) 415 bp cohesive end fragment with 10 mM $MgCl_2$. The arrows indicate the presence of circular molecules absent of (B) 441 bp blunt end fragment that were also incubated in 10 mM $MgCl_2$. Present within panel A are linear and circular monomers along with linear dimers and trimers. Zoomed image of (C) linear monomer, (D) circular monomer, (E) linear dimer, and (F) linear trimer of the 415 bp cohesive end fragment. (G) 415 bp cohesive end fragment incubated with 200 mM NaCl.

μL of sample was deposited on mica that was functionalized by aminopropylsilatrane (APS-mica) using the protocol described earlier (*9*). After 2 min, samples were rinsed with deionized water (ModuPure Plus, Continental Water System Corp., San Antonio, TX) and argon-dried.

AFM Analysis. AFM images were obtained with MultiMode SPM instrument equipped with an E-scanner (Digital Instruments, San Barbara, CA) operating in Tapping Mode as described elsewhere (*9*−*11*). Conical sharp silicon tips (K-TEK international, Portland, OR) were used for imaging in air, and tapping frequencies were in the range of 350−440 kHz and the scan rate 3.05 Hz (*10*).

Analysis of AFM Data. Femtoscan Online v 1.6 (4.4) (Moscow State University and Advanced Technologies Center, Moscow, Russia) was used for measurements of contour length and end-to-end distances of DNA fragments. The number of molecules analyzed per sample was approximately 100. Statistical analysis of data was performed on both Kaleidagraph v 3.0.1 (*10*) and Excel 2000 software (Microsoft).

RESULTS

AFM Images of the cohesive end fragment in the presence of 10 mM $MgCl_2$ deposited on APS-mica are shown in Figure 1A. The striking feature of these images is the appearance of circular molecules. A few of them are indicated with arrows in Figure 1A. The number of the circles drops for the sample prepared at low concentration of Mg^{2+} (Figure 2B and data not shown), and no circles are formed for the 441 bp fragment with blunt ends prepared in 10 mM of $MgCl_2$ (Figure 1C). These data show that cohesive ends are involved in the circles formation. Therefore, we should also expect to see linear oligomers in addition to circles formed. We indeed observed Mg^{2+}-induced oligomerization of the fragment, and a few examples of zoomed images are shown in Figure 1C−F. Using these zoomed images, we

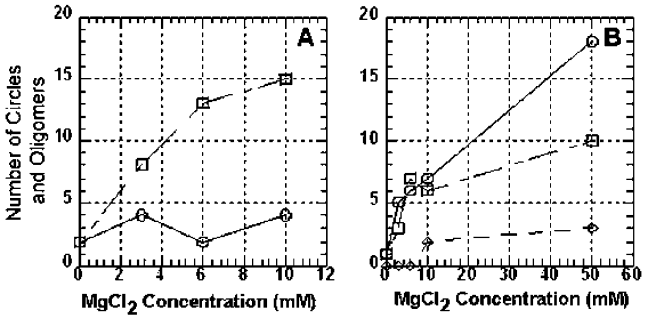

FIGURE 2: Total circle formation and oligomerization of all DNA fragments as a function of $MgCl_2$ concentration. (A) (□) Corresponds to the 415 bp blunt end fragment, and (○) corresponds to the 415 bp cohesive end fragment and the 441 bp blunt end fragment is absent since no circles or oligomers were detected. (B) 415 bp cohesive end fragment analysis of the frequencies of (○) circles, (□) linear dimers, and (◇) linear trimers as a function of $MgCl_2$ concentration (0, 3, 6, 10, and 50 mM). (Approximately 100 molecules were analyzed per sample.)

classified circles and oligomers of the linear cohesive end fragments based on linear and circular monomers as shown in panels C and D, respectfully, of Figure 1 and linear dimers and trimers as shown panels E and F, respectfully. We further characterized end stability as a function of Mg^{2+} concentration by using this classification scheme and comparing the yield of each fragment (Figure 2A). Again, the data illustrate that the fragment with cohesive ends has a significantly higher yield of circles and oligomers than either blunt end fragment (Figure 2A). Additionally, further analysis of the cohesive end fragment was done using this classification scheme. The results show that in all cases, linear circles, dimers, and trimers all appear to increase as the amount of Mg^{2+} increases (Figure 2B).

To further characterize the effect of Mg^{2+} concentration on circle formation, the end-to-end distance was measured for approximately 100 molecules in each sample, and the histograms illustrating these data are shown in Figure 3. These data show clearly that Mg^{2+} cations dramatically change the end-to-end distance distribution. The population of molecules with small end-to-end distances increases as the Mg^{2+} concentration increases, and this eventually leads to the formation of bimodal distributions at elevated concentrations of Mg^{2+} (Figure 3C and D). Thus, the measurements of the end-to-end distances is a another clear characteristic of the effect of Mg^{2+} on the conformation of DNA fragments with cohesive ends illustrated by AFM images in Figure 1A.

To determine whether this effect of Mg^{2+} observed with cohesive end and blunt end fragments is purely due to electrostatics, we compared the effect of Mg^{2+} cations with Na^+, using the latter in a 20-fold greater concentration (*12*). An AFM image of the cohesive end fragment prepared with 200 mM NaCl is shown in Figure 1G. There are few circular fragments on the field, but the effect is much less than that in 10 mM $MgCl_2$. In fact, the population of circles and oligomers is reduced 5-fold for the sample incubated with NaCl as compared that to with $MgCl_2$ (data not shown). These data suggest that a mechanism other than pure electrostatics is responsible for the stabilization effect of Mg^{2+} on the hybridization of cohesive ends.

Mg^{2+} Effects Compared to Other Divalent Cations. To further determine if the effect of cohesive end stabilization

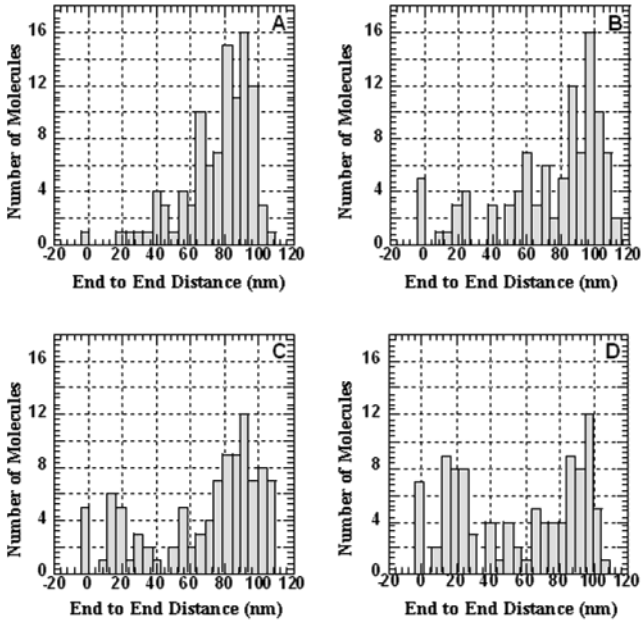

FIGURE 3: End-to-end distance measurements of the 415 bp cohesive end fragments as a function of $MgCl_2$ concentration for (A) 0 mM $MgCl_2$, (B) 3 mM $MgCl_2$, (C) 6 mM $MgCl_2$, and (D) 10 mM $MgCl_2$. Approximately 100 monomer molecules were analyzed per sample.

is specific to Mg^{2+} and to shed light on what the specific interactions are with the ends, we incubated the 415 bp cohesive end fragment with various concentrations of Ca^{2+}, Mn^{2+}, and Zn^{2+}. All divalent cations produced circularized molecules and oligomers, as were observed with Mg^{2+} (data not shown). The dependence of circle and oligomer formation on cation concentration is plotted in Figure 7. The data show that Ca^{2+} and Mn^{2+} behaved similarly with Mg^{2+} (Figure 7A−C) but Zn^{2+} produced substantially more circularized molecules (Figure 7D). Interestingly, Zn^{2+} samples showed that as the concentration of $ZnCl_2$ was increased from 0 to 10 mM, the amount of isolated molecules on the surface were dramatically reduced in comparison with the sample with no Zn^{2+} (Figure 8A,B). We found that 10 mM $ZnCl_2$ induces the formation of large aggregates such as shown in Figure 8F (inset images). We suggest that this dramatic reduction in the number of isolated DNA molecules in the presence of 10 mM $ZnCl_2$ was due to this Zn^{2+} induced aggregation. Additionally, at this concentration of Zn^{2+}, other interesting molecules were observed. In Figure 8D,E, inset images show Zn^{2+}-induced circles of different morphologies that are absent in the other divalent cation samples.

Effect of Mg^{2+} on DNA Flexibility. To distinguish between the effects of Mg^{2+} on the cohesive ends stability (local effect) from the possible effect on DNA flexibility (global DNA structure effect), we performed the studies with DNA fragments with blunt ends. We did not observe the formation of circles with the 441 bp fragment (Figure 1B) and very few with the 415 bp blunt end fragment (image not shown). We used end-to-end distance measurements to estimate a possible contribution of Mg^{2+} to DNA flexibility (*13*−*15*). To rule out sequence effects on DNA flexibility, two DNA fragments with approximately similar lengths but different sequences were investigated. The end-to-end distances for the 441 bp fragment prepared with various $MgCl_2$ concentrations were measured and the data plotted as histograms

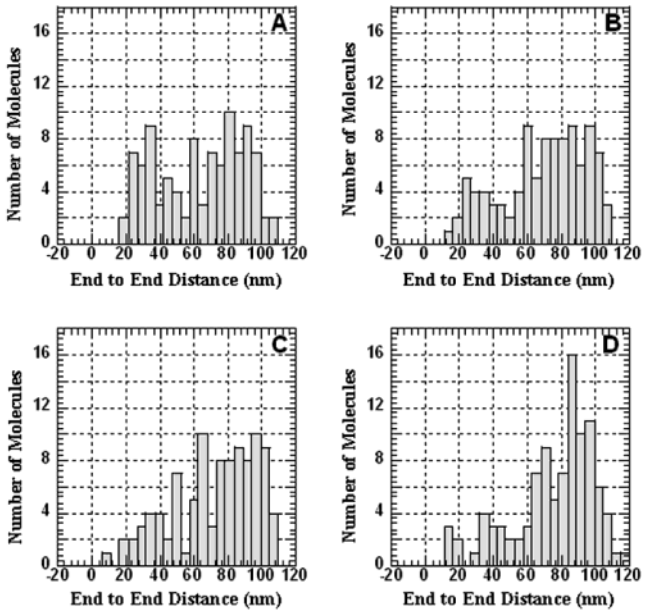

FIGURE 4: End-to-end distance measurements of the 441 bp blunt end fragments as a function of $MgCl_2$ concentration. (A) 0 mM $MgCl_2$, (B) 3 mM $MgCl_2$, (C) 6 mM $MgCl_2$, (D) 10 mM $MgCl_2$. Approximately 100 monomer molecules were analyzed per sample.

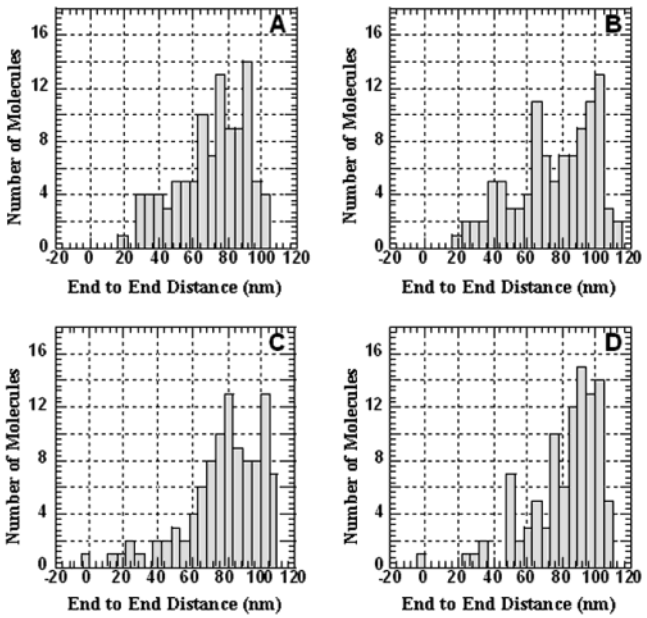

FIGURE 5: End-to-end distance measurements of the 415 bp blunt end fragments as a function of $MgCl_2$ concentration for (A) 0 mM $MgCl_2$, (B) 3 mM $MgCl_2$, (C) 6 mM $MgCl_2$, and (D) 10 mM $MgCl_2$. Approximately 100 monomer molecules were analyzed per sample.

(Figure 4). Initially a broad and clearly bimodal distribution obtained in the absence of Mg^{2+} cations is transformed to an asymmetric distribution upon adding Mg^{2+}. This DNA fragment contains a 60-bp long track of alternating (C,A) repeats that according to NMR (*16*), cyclization (*17*−*19*), and crystallographic data (*20*, *21*) exhibit elevated flexibility. This insert is located $\sim^1/_3$ from its end of the length of the fragment, and elevated flexibility may lead to the formation of a population of rather curved molecules. Interestingly, the elevated flexibility is eliminated with the addition of Mg^{2+} cations that lead to a rather asymmetric distribution for the end-to-end distance.

Both of the 415 bp fragments are intrinsically curved due to the inherent curvature of a Fis protein binding site that contains several A-tracts that are located in the middle of the blunt end fragment and near one end of the cohesive end fragment (*22*). To compare the effect of the CA element to that of the Fis protein binding site, a similar analysis was performed on the 415 bp blunt end fragment (Figure 5). The distribution for the sample prepared without $MgCl_2$ (Figure 5A) is dramatically different from that for the 441 bp fragment (Figure 4A), illustrating clearly the effect of the (C,A) repeats on DNA flexibility. The addition of $MgCl_2$ does not lead to significant changes in the distribution except for a slight shift of the maximum toward larger lengths. This effect is illustrated graphically in Figure 6, where the mean end-to-end distances are plotted versus Mg^{2+} concentration. The large error bars are due to a rather broad distribution, but despite a large standard deviation, there is a clear trend toward the slight increase of end-to-end distance with Mg^{2+} concentration.

It is constructive to compare these results with the combined effects of Mg^{2+} on the stability of the sticky ends and on overall DNA flexibility (local and global effects respectively). The latter effect can be characterized by the mean end-to-end distance. These values for the fragment with cohesive ends (Figure 3) are also plotted in Figure 6A. The

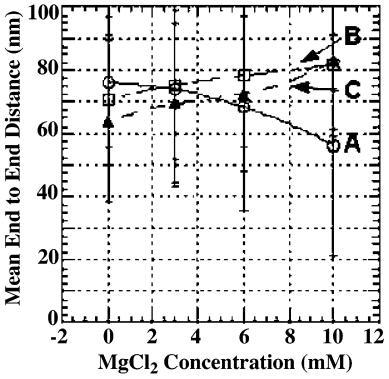

FIGURE 6: Mean end-to-end distance of all DNA fragments as a function of $MgCl_2$ concentration. (A) The mean end-to-end distance for the (○) 415 bp cohesive end fragment calculated from Figure 3. (B) The mean end-to-end distance for the (▲) 415 bp blunt end fragment calculated from Figure 5. (C) The mean end-to-end distance for the (□) 441 bp blunt end fragment calculated from Figure 4. Each error bar (for all symbols) represents the standard deviation for each corresponding data point.

cumulative effect of Mg^{2+} is a drop end-to-end distance with increasing Mg^{2+} concentration. At the same time, the data for both blunt end fragments are opposite where the effect is a slight increase in the end-to-end distance as a function of Mg^{2+} concentration (Figure 6B and C). These data suggest that Mg-mediated cyclization effect for the fragments with overhanging ends is solely due to the stabilization of complementary regions by the cations.

DISCUSSION

Effect of Stabilization of the Cohesive Ends As A Function Mg^{2+} and Other Divalent Cations. Our results show that fragments containing cohesive ends have an increased propensity of transient circle formation in the presence of Mg^{2+}. We noticed a 7.5-fold increase in the formation of circles and oligomers for the fragment containing cohesive ends when the $MgCl_2$ concentration was increased from 0

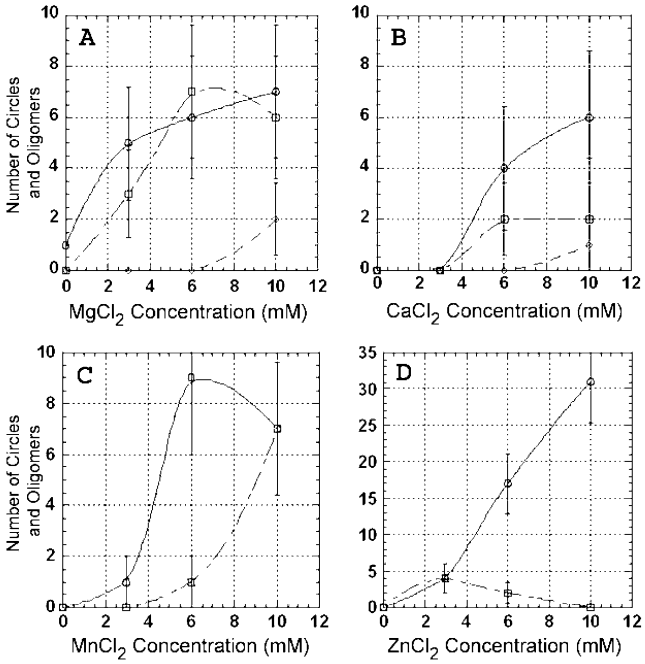

FIGURE 7: Total circle formation and oligomerization of the 415 bp cohesive end fragment as a function of divalent cation (Mg^{2+}, Ca^{2+}, Mn^{2+}, and Zn^{2+}) concentration. (A−D) 415 bp cohesive end fragment analysis of the frequencies of (○) circles, (□) linear dimers, and (◇) linear trimers as a function of divalent cation concentration (0, 3, 6, and 10 mM). (A) $MgCl_2$, (B) $CaCl_2$, (C) $MnCl_2$, (D) $ZnCl_2$. (Approximately 100 molecules were analyzed per sample and included is Poisson statistical error [$\sqrt{\#}$].)

to 10 mM and an additional 2-fold increase when Mg^{2+} was increased to 50 mM (Figure 2B). These data indicate a link between the concentration of Mg^{2+} and the end stability of cohesive end fragments. This effect of Mg^{2+} is not simply due to electrostatic screening of Mg^{2+}on the DNA backbone. If this were the case, Mg^{2+} could be substituted with Na^{+}; we did not observe the formation of circles at a comparable concentration of NaCl (10 mM $MgCl_2$ vs 50 mM NaCl). Even a 20-fold higher concentration of NaCl was not sufficient to approach the effect of 10 mM $MgCl_2$ on the formation of circles (*12*). In the presence of 200 mM Na^{+}, the end stability seen with 10 mM Mg^{2+} is lost (Figure 1G). These data confirm that Mg^{2+} is needed for complementary end-strand stabilization, as proposed by Révet and Fourcade (*8*). Our data show that the effect depends on the Mg^{2+} concentration so that the yield of circles approaches 18% at 50 mM $MgCl_2$ solution. It would appear that Mg^{2+} acts as some sort of stabilizing zipper that helps stabilize complementary base pairing within cohesive ends. Furthermore, this zipper could be achieved when hydrated magnesium ions act as a pseudobase by donating hydrogen bonds through associated water molecules (*23*) when two complementary single stranded ends come in close proximity (<10 nm).

Our results further showed that other cations (Ca^{2+} and Mn^{2+}) display similar effects to that of Mg^{2+}, which further suggests these cations function in a similar manner. We further showed that the cyclization of the 415 bp cohesive end fragment in the presence of increasing concentrations of $ZnCl_2$ was substantially greater than that with Mg^{2+} (Figure 7A,D). Under these conditions Zn^{2+} stabilizes end-to-end interaction much more efficiently than Mg^{2+}. In addition, at the highest concentration of $ZnCl_2$ we observed DNA aggregation (Figure 8F) (*6*) that was not previously observed with the other divalent cations investigated here. These data suggest that Zn^{2+} might have a stronger interaction with bases than Mg^{2+} and further promote base−base hybridization. Although acidic conditions were used to avoid the formation of insoluble $Zn(OH)_2$ (*24*), the effect observed with Zn^{2+} are not a consequence of the acidic buffer. When the fragments were incubated in this buffer in the absence of $ZnCl_2$, there was no noticeable difference when compared to the other controls (Figure 8A and data not shown). DNA aggregation mediated by Zn^{2+} was reported earlier (*6*, *25*).

Effect of Mg^{2+} on DNA Flexibility. Our AFM measurements of the end-to-end distance (Figure 6) show that this parameter decreases as the Mg^{2+} concentration increases. These data suggest that Mg^{2+} increases DNA flexibility,

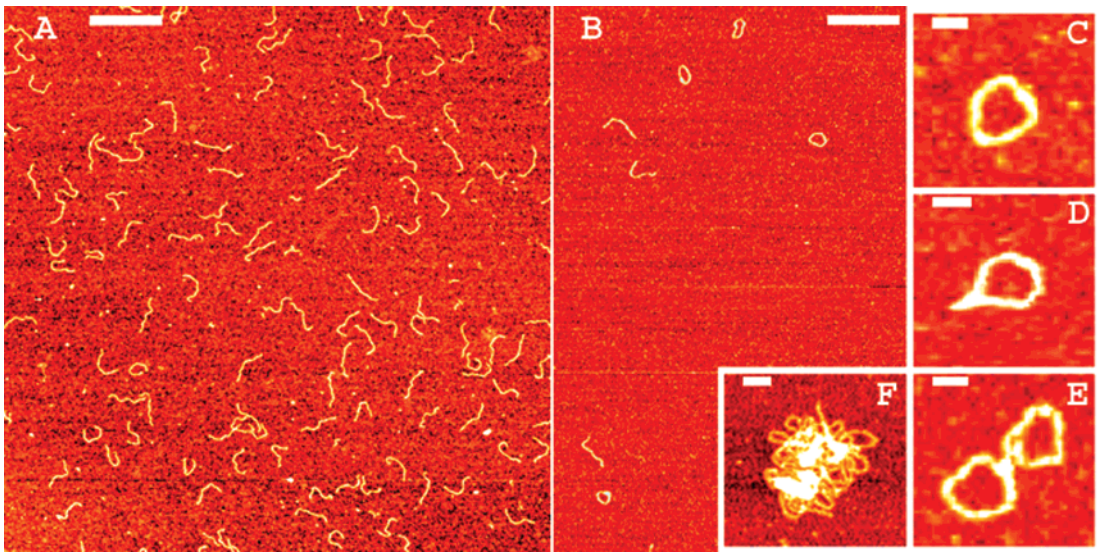

FIGURE 8: AFM images showing the effects of Zn^{2+} on cohesive end stabilization. (A) 415 bp cohesive end fragment incubated in the absence of $ZnCl_2$. (B) 415 bp cohesive end fragment incubated in the presence of 10 mM $ZnCl_2$. The inset images are zoomed images of (C) a circularized fragment, (D) a circularized fragment with the ends in a parallel orientation, (E) two interacting fragments of interesting morphology, and (F) aggregation of fragments induced by Zn^{2+}. (Scales are as follows: (A and B) 200 nm, (C and D) 20 nm, (E) 40 nm, and (F) 60 nm.)

although the effect is rather weak. This conclusion is supported by the majority of experimental data obtained by DNA ring closure (*26*), molecular dynamic simulations (*27*, *28*), and various experimental approaches [for review 29 ref. therein], which show little or no effect of Mg^{2+} on DNA flexibility. It should be noted that we observed a slight reduction in DNA flexibility for both the 415 and 441 bp blunt end fragments, corroborating a small increase of mean end-to-end distance (Figure 6B,C), which was also observed previously (*26*). Conversely, recent force spectroscopy studies (*30*, *31*) and molecular dynamic simulations (*32*) suggest that Mg^{2+} increases DNA flexibility. Our data do not support this finding, and conflicting results may lie in the differences in experimental approaches used to investigate the problem.

Comparison of these results with the end-to-end distance measurements of the fragments with self-complementary ends clearly indicates that the effect of Mg^{2+} is a consequence of cohesive end stabilization. This is apparent in the growth of the population of molecules with small end-to-end distances ($<$30 nm) for the cohesive end fragment with increasing Mg^{2+} (Figure 3). A fraction of this population is composed of circular molecules that are distinguished by having end-to-end distances of zero, and we suggest that the remainders are a result of the dynamic process of cyclization. When these circular molecules are formed, they are stabilized in the presence of Mg^{2+}, but they are not covalently closed. Although Mg^{2+} stabilizes end-to-end interactions, it is likely that a dynamic equilibrium is present between linear and circular fragments (*33*).

Furthermore, we examined the possible effects of Mg^{2+} with specific sequence elements in the fragments. The 441 bp blunt end fragment, which contains a 60 bp CA repeats, exhibits what appears to be intrinsic dynamic flexibility in the absence of Mg^{2+} (Figure 4A), but as the amount of Mg^{2+} increases, the appearance of molecules with short end-to-end distances decreases (Figure 4B−D). It has been shown earlier that DNA containing CA elements exhibits unusual sequence flexibility, and moreover it can adopt different DNA conformations (*7*, *17*, *20*, *21*, *34*). Thus, the CA element may be undergoing a DNA conformational shift driven by increasing Mg^{2+}, which could explain the decrease in DNA flexibility. Similar to the 441 bp fragment, both 415 bp fragments exhibit changes in their flexibility in the presence of increasing Mg^{2+}. Like the 441 bp fragment, both blunt and cohesive end 415 bp fragments contain a Fis site, a flexible insert made up of several A-tracts, which could influence their overall flexibility (*35*). Thus, DNA fragments that contained A-tracts will exhibit static bends or curvature, and these are accentuated in the presence of monovalent and divalent cations (*5*, *7*). Furthermore, the position of the Fis site within these 415 bp fragments may affect the overall degrees of curvature (*22*). We would expect on the basis of the position of the Fis site that the 415 bp blunt end fragment would exhibit a higher degree of curvature compared to the 415 bp cohesive end fragment (ignoring the end effect). Additionally, in the presence of Mg^{2+}, both fragments should be affected in a same manner since they contain the identical Fis site. Interestingly, we observed the decrease in curvature with increasing Mg^{2+} within the blunt end fragment, whereas we observed just the opposite for the cohesive end (Figure 6A,C). And when both 415 bp fragments were each incubated with a 20-fold excess of Na^{+}, their results were similar (data not shown). These results are most interesting due to the fact that both 415 bp fragments (blunt and cohesive end) are identical in length and base composition, and the fragment that the Fis site was cloned into contains no detectable bends (*36*). The main differences between these 415 bp fragments are the position of the Fis site and the type of ends they have.

This observed effect of Mg^{2+} on DNA fragments has several implications with regards to enzymes involved in repair and management of DNA fragments. Ligases, among many enzymes, rely on Mg^{2+} as a cofactor, but our study suggests that ligation may also be dependent upon the role of Mg^{2+} in complementary strand hybridization.

ACKNOWLEDGMENT

The authors would like to thank Dr. S. Levene for useful comments and Chad McAllister for critical reading and comments on the manuscript. We would also like to thank Dr. R. Johnson and Dr. V. Potaman for providing us with plasmid pRJ1199 and Dr. Strauss for the 441 bp fragment.

REFERENCES

1. Lilley, D. M. (2000) Structures of helical junctions in nucleic acids, *Q Rev. Biophys. 33* (2), 109−59.
2. Welch, J. B., Duckett, D. R., and Lilley, D. M. (1993) Structures of bulged three-way DNA junctions, *Nucleic. Acids. Res. 21* (19), 4548−55.
3. Soyfer, V. N., and Potaman, V. N. (1996) *Triple-Helical Nucleic Acids*, p 360, Springer, New York.
4. Brukner, I., et al. (1994) Physiological concentration of magnesium ions induces a strong macroscopic curvature in GGGCCC-containing DNA, *J. Mol. Biol. 236* (1), 26−32.
5. Diekmann, S. (1987) Temperature and salt dependence of the gel migration anomaly of curved DNA fragments, *Nucleic. Acids. Res. 15* (1), 247−65.
6. Laundon, C. H., and Griffith, J. D. (1987) Cationic metals promote sequence-directed DNA bending, *Biochemistry 26* (13), 3759−62.
7. Shlyakhtenko, L. S., et al. (1990) Influence of Temperature and Ionic Strength on Electrophoretic Mobility of Strength DNA Fragments, *Mol. Biol. 24* (1), 79−95.
8. Revet, B., and Fourcade, A. (1998) Short unligated sticky ends enable the observation of circularised DNA by atomic force and electron microscopies, *Nucleic. Acids Res. 26* (9), 2092−2097.
9. Shlyakhtenko, L. S., et al. (2000) Structure and dynamics of three-way DNA junctions: atomic force microscopy studies, *Nucleic. Acids Res. 28* (18), 3472−3477.
10. Oussatcheva, E. A., et al. (1999) Structure of branched DNA molecules: Gel retardation and atomic force microscopy studies, *J. Mol. Biol. 292* (1), 75−86.
11. Shlyakhtenko, L. S., et al. (1998) Structure and dynamics of supercoil-stabilized DNA cruciforms, *J. Mol. Biol. 280* (1), 61−72.
12. Shaw, S. Y., and Wang, J. C. (1993) Knotting of a DNA Chain During Ring-Closure, *Science 260* (5107), 533−536.
13. Hansma, H. G., and et al. (1994) Bending and Straightening of DNA Induced by Same Ligand: Characterization with the Atomic Force Microscope, *Biochemistry 33*, 8436−8441.
14. Rivetti, C., Guthold, M., and Bustamante, C. (1996) Scanning force microscopy of DNA deposited onto mica: equilibration versus kinetic trapping studied by statistical polymer chain analysis, *J. Mol. Biol. 264* (5), 919−32.
15. Rivetti, C., Walker, C., and Bustamante, C. (1998) Polymer chain statistics and conformational analysis of DNA molecules with bends or sections of different flexibility, *J. Mol. Biol. 280* (1), 41−59.
16. Russu, I. M. (1991) Studying DNA-Protein Interactions Using Nmr, *Trends Biotechnol. 9* (3), 96−104.
17. Lyubchenko, Y. L., et al. (1993) Ca Runs Increase DNA Flexibility in the Complex of Lambda-Cro Protein with the Or3 Site, *Biochemistry 32* (15), 4121−4127.

18. Lyubchenko, Y., et al. (1991) DNA Bending Induced by Cro Protein-Binding as Demonstrated by Gel-Electrophoresis, *Proc. Natl. Acad. Sci. U.S.A. 88* (12), 5331−5334.
19. Lyubchenko, Y. L., et al. (1993) Alternating Pyrimidine-Purine Sequences Increase DNA Flexibility in the Complex between Cro Protein and the Lambda- Or3 Binding-Site, *Biophys. J., 64* (2), A179−A179.
20. Timsit, Y., Vilbois, E., and Moras, D. (1991) Base-Pairing Shift in the Major Groove of (Ca)N Tracts by B-DNA Crystal-Structures, *Nature 354* (6349), 167−170.
21. Timsit, Y., et al. (1989) Unusual helical packing in crystals of DNA bearing a mutation hot spot, *Nature 341* (6241), 459−62.
22. Pan, C. Q., et al. (1996) Variable structures of Fis-DNA complexes determined by flanking DNA-protein contacts. *J. Mol. Biol. 264* (4), 675−695.
23. Petrov, A. S., Lamm, G., and Pack, G. R. (2002) Water-mediated magnesium-guanine interactions, *J. Phys. Chem. B 106* (12), 3294−3300.
24. Thomson, N. H., et al. (1996) Reversible binding of DNA to mica for AFM imaging, *Langmuir* 12 (*24*), 5905−5908.
25. Ortizlombardia, M., et al. (1995) Divalent Zinc Cations Induce the Formation of 2 Distinct Homoduplexes of a D(Ga)(20) DNA-Sequence, *Biochemistry 34* (44), 14408−14415.
26. Taylor, W. H., and Hagerman, P. J. (1990) Application of the method of phage T4 DNA ligase-catalyzed ring-closure to the study of DNA structure. II. NaCl-dependence of DNA flexibility and helical repeat, *J. Mol. Biol. 212* (2), 363−76.
27. Hagerman, P. J., and Ramadevi, V. A. (1900) Application of the method of phage T4 DNA ligase-catalyzed ring-closure to the study of DNA structure. I. Computational analysis. *J. Mol. Biol. 212* (2), 351−62.
28. Hagerman, P. J. (1983) Electrostatic Contribution to the Stiffness of DNA-Molecules of Finite Length, *Biopolymers 22* (3), 811−814.
29. Hagerman, P. J. (1988) Flexibility of DNA, *Annu. Rev. Biophys. Biophys. Chem. 17*, 265−286.
30. Baumann, C. G., et al. (1998) The ionic strength dependence of the DNA overstretch force indicates a narrow fiber DNA conformation, *Biophys. J. 74* (2), A284−A284.
31. Baumann, C. G., et al. (1997) Ionic effects on the elasticity of single DNA molecules, *Proc. Natl. Acad. Sci. U.S.A. 94* (12), 6185−6190.
32. Rouzina, I., and Bloomfield, V. A. (1998) DNA bending by small, mobile multivalent cations. *Biophys. J. 74* (6), 3152−3164.
33. Shore, D., Langowski, J., and Baldwin, R. L. (1981) DNA Flexibility Studied by Covalent Closure of Short Fragments into Circles, *Proc. Natl. Acad. Sci. U.S.A.—Biol. Sci. 78* (8), 4833−4837.
34. Gaillard, C., and Strauss, F. (1994) Association of poly(CA)·poly-(TG) DNA fragments into four-stranded complexes bound by HMG1 and 2, *Science 264* (5157), 433−6.
35. Sinden, R. R. (1994) *DNA Structure and Function*, p 393, San Diego, Academic Press.
36. Prentki, P., Pham, M. H., and Galas, D. J. (1987) Plasmid Permutation Vectors to Monitor DNA Bending, *Nucleic. Acids Res. 15* (23), 10060−10060.

BI026102E